Available online at www.sciencedirect.com

SCIENCE DIRECT®

ELSEVIER

Journal of Contaminant Hydrology 83 (2006) 70–88

JOURNAL OF Contaminant Hydrology

www.elsevier.com/locate/jconhyd

The effect of silica on the degradation of organohalides in granular iron columns

Tamar Kohn, A. Lynn Roberts *

Department of Geography and Environmental Engineering, 313 Ames Hall Johns Hopkins University, 3400 N. Charles St., Baltimore, MD 21218-2686, USA

Received 7 June 2004; received in revised form 14 October 2005; accepted 20 October 2005
Available online 20 December 2005

Abstract

Dissolved silica species are naturally occurring, ubiquitous groundwater constituents with corrosion-inhibiting properties. Their influence on the performance and longevity of iron-based permeable reactive barriers for treatment of organohalides was investigated through long-term column studies using Connelly iron as the reactive medium. Addition of dissolved silica (0.5 mM) to the column feed solution led to a reduction in iron reactivity of 65% for trichloroethylene (TCE), 74% for 1,1,2-trichloroethane (1,1,2-TCA), and 93% for 1,1,1-trichloroethane (1,1,1-TCA), compared to columns operated under silica-free conditions. Even though silica adsorption was a gradual process, the inhibitory effect was evident within the first week, with subsequent decreases in reactivity over 288 days being relatively minor. Lower concentrations of dissolved silica species (0.2 mM) led to a lesser decrease (70%) in iron reactivity toward 1,1,1-TCA. The presence of dissolved silica species produced a shift in TCE product distribution toward the more highly chlorinated product *cis*-dichloroethylene (*cis*-DCE), although it did not appear to alter products originating from the trichloroethanes. The major corrosion products identified were magnetite (Fe_3O_4) or maghemite (γ-Fe_2O_3) and carbonate green rust ($[Fe_4^{2+}Fe_2^{3+}(OH)_{12}][CO_3 \cdot 2H_2O]$). Iron carbonate hydroxide ($Fe(II)_{1.8}Fe(III)_{0.2}(OH)_{2.2}CO_3$) was only found in the silica-free column, indicating that silica may hinder its formation. A comparison with columns operated under the same conditions, but using Master Builder iron as the reactive matrix, showed that Connelly iron is initially less reactive, but performs better than Master Builder iron over 288 days.

Keywords: Silica; Connelly iron; Column study; Trichloroethane; Trichloroethylene; Precipitate characterization

* Corresponding author. Tel.: +1 410 516 4387; fax: +1 410 516 8996.
E-mail address: lroberts@jhu.edu (A. Lynn Roberts).

0169-7722/$ - see front matter © 2005 Elsevier B.V. All rights reserved.
doi:10.1016/j.jconhyd.2005.10.010

1. Introduction

Since their first implementation a decade ago, iron-based permeable reactive barriers (PRBs) have established themselves as a successful technology for treating some of the most frequently encountered groundwater pollutants. Because of their novelty, some concerns regarding the longevity of PRBs still remain. In particular, the influence of groundwater composition on PRB performance has yet to be fully addressed.

When groundwater passes through an iron-based PRB, contaminants such as chlorinated solvents or nitroaromatic compounds undergo reduction by the iron matrix in a corrosion-like process (Gillham and O'Hannesin, 1994; Agrawal and Tratnyek, 1996), whereas several oxyanions such as arsenate or chromate, as well as metals and radionuclides, may be immobilized by (in some cases reductive) adsorption to the iron matrix and newly formed iron (hydr)oxide phases, or by (reductive) precipitation (Cantrell et al., 1995; Blowes et al., 1997; Gu et al., 1998; Su and Puls, 2001a; Wilkin and McNeil, 2003). The long-term success of a PRB is thus dictated by its ability to sustain a high level of corrosion activity over time, in order to provide electrons for contaminant reduction or to generate fresh iron (hydr)oxide corrosion products as a continuous source of adsorption sites.

Naturally occurring groundwater constituents such as silica species, phosphate or carbonate, as well as co-contaminants such as chromate or nitrate in mixed contaminant plumes, have been shown (Deng et al., 1998; Schlicker et al., 2000; Klausen et al., 2001, 2003; Su and Puls, 2001b, 2003; Kohn et al., 2003; Ritter et al., 2003) to exert a detrimental effect on the reactivity of the iron matrix. Silica species are ubiquitous solutes in groundwater, and are well-known corrosion inhibitors that readily adsorb onto iron (hydr)oxides (Sigg and Stumm, 1981; Swedlund and Webster, 1999; Sass et al., 2001; Kohn et al., 2003); their total concentration in groundwater typically lies between 0.12 and 0.75 mM (Davies et al., 2002). Batch studies conducted by Su and Puls (2001b) demonstrated that silica species decrease the rate of arsenate (As(V)) and arsenite (As(III)) removal from aqueous solution by Peerless iron. In a later column study using Peerless iron, sand and sediment as the reactive matrix, Su and Puls (2003) further showed that the combination of phosphate and silica species in the feed solution resulted in earlier breakthrough of total dissolved As compared to silica- and phosphate-free columns. Deng et al. (1998) found a detrimental effect of silica species toward the degradation of trichloroethylene (TCE) by iron particles in batch studies. Klausen et al. (2001) showed that the presence of silica species in the feed solution greatly diminished the rate of reduction of nitroaromatic compounds in columns packed with Master Builder iron. Previous column studies performed in our laboratory also indicated that a short-term addition of silica species had an inhibitory effect on the reactivity of Master Builder iron toward TCE and nitroaromatic compounds (Klausen et al., 2003). Recent batch studies using electrolytic iron (Kohn et al., 2003) revealed that the decrease in iron reactivity toward 1,1,1-trichloroethane (1,1,1-TCA) is a function of solution pH, silica loading, and exposure time of the iron to silica-containing solutions.

Even though the inhibitory effect of silica on iron reactivity was recognized in these studies, to date no column studies have explored the influence of sustained exposure to dissolved silica species on the reactivity of iron toward organohalides. Furthermore, little attention has been given to differences in the influence of silica species on different classes of organohalides (i.e., alkyl versus vinyl halides), to the effect of silica on the distribution of products arising from organohalide reduction, or to silica's influence on the identity of (hydr)oxide phases that develop.

The inhibitory effect of silica on iron reactivity can be attributed to physical and chemical factors. Su and Puls (2001b) ascribe the diminished removal of As species to competition by silica species for sorption sites on iron (hydr)oxides. Silica sorption could either physically block access of the contaminants to the reactive sites, or it could chemically alter the reactivity of the interfacial region by changing the speciation of the surface-associated iron. Surface-associated iron can be viewed as an ionic interaction between a metal ion and the corrosion products, or as iron incorporated in the corrosion product(s). For redox-active compounds, the decrease in iron reactivity could also be explained by the tendency of silica to serve as an anodic corrosion inhibitor that prevents the iron from releasing electrons to the contaminants (Sastri, 1998). This may in part result from formation of a protective layer, consisting of a hydrated silica gel/metal oxide crust that forms a physical barrier between the iron and the contaminants. Redox-active corrosion products such as magnetite (Fe_3O_4) or green rust (e.g., $[Fe_4^{2+}Fe_2^{3+}(OH)_{12}][CO_3 \cdot 2H_2O]$) may play important roles in contaminant reduction, thereby helping to maintain the reactivity of PRBs (Klausen et al., 1995; Sivavec and Horney, 1997; Erbs et al., 1999; Williams and Scherer, 2001; Lee and Batchelor, 2002a,b; O'Loughlin et al., 2003). The presence of dissolved silica species has been shown (Anderson and Benjamin, 1985; Hansen et al., 1994; Mayer and Jarrell, 1996) to alter the types of iron (hydr)oxide phases that may form. A shift in precipitate identity to less redox active phases or phases with fewer sorption sites could potentially reduce PRB efficacy.

In this study we report on the first systematic long-term column experiments to monitor the effect of silica species on iron reactivity toward chlorinated solvents, compared to silica-free systems. The objectives were to determine the influence of silica on the rate of degradation of TCE, 1,1,1-TCA and 1,1,2-trichloroethane (1,1,2-TCA) over time, as well as to examine any shifts in product distribution that might occur. We also investigated the effect of dissolved silica on the precipitates formed in columns, using scanning electron microscopy and X-ray diffraction.

Different types of iron exhibit different reactivities toward TCE (Su and Puls, 1999). Connelly iron was selected for the present study because this material is currently used for the majority of iron-based PRBs within the US (Connelly-GPN, 2004). This material is an impure cast iron product, in which granules are covered by an iron oxide layer formed during a high-temperature oxidation process (Ritter et al., 2002). Because the silica-free column experiment in the present study was performed under conditions identical to previous column studies conducted in our laboratory using a different commercial iron, Master Builder iron, direct comparison between the longevity of two types of cast iron in silica-free systems was also possible.

2. Materials and methods

2.1. Chemicals

Inorganic feed solutions were prepared from sodium bicarbonate ($NaHCO_3$, J.T. Baker), sodium hydroxide pellets (NaOH, J.T. Baker), and sodium metasilicate nonahydrate ($Na_2SiO_3 \cdot 9H_2O$, Sigma) in deionized water. Contaminant stock solutions of 1,1,1-trichloroethane (1,1,1-TCA, 99.5%, Aldrich), 1,1,2-trichloroethane (1,1,2-TCA, 98%, Aldrich), trichloroethylene (TCE, 98%, Aldrich) and *cis*-dichloroethylene (*cis*-DCE, 98%, Aldrich) were prepared in deaerated 50% methanol (HPLC grade, J.T. Baker)/50% deionized water. For product identification and quantification, aqueous standards were prepared from 1,1,1-TCA, 1,1,2-TCA, TCE, *cis*-DCE, trans-dichloroethylene (trans-DCE, 98%, Aldrich), 1,1-dichloroethy-

lene (1,1-DCE, 99%, Aldrich), 1,1-dichloroethane (1,1-DCA, 99%, TCI America), vinyl chloride (VC, 2000 μg/mL in methanol, Supelco), 2-butyne (99%, Aldrich), as well as by dissolving the gaseous species ethane, ethylene and *cis*-2-butene (using gas standards purchased from Scott Specialty Gases) in deionized water. Iron filings were obtained from Connelly-GPM, Inc. (Chigaco, IL).

2.2. Column description and operation

Experiments were carried out in four Plexiglas columns (39 cm × 3 cm ID) containing a Connelly iron matrix. The iron was sieved to obtain grains ranging from 360 μm to 1.4 mm in diameter. The columns were equipped with 14 stainless steel liquid sampling ports, and three ports for the extraction of solid samples (one near the influent, one in the middle and one near the effluent of every column). The exact dimensions of the columns and positions of the sampling ports are as described in our prior column studies (Vikesland et al., 2003).

Feed solutions containing 2 mM $NaHCO_3$ were stored in polypropylene containers that were continuously sparged with N_2 to exclude oxygen. The feed solutions for Columns 2 and 4 also contained 0.5 mM dissolved silica species. A lower concentration of dissolved silica species (0.2 mM) was added to the feed solution of Column 3 near the end of the experiments, from day 210 to day 273. Stock solutions (1:1 water/methanol solvent) containing the contaminants were stored in 50 mL gas-tight syringes.

The inorganic feed solutions were pumped into 60 mL mixing chambers by means of a peristaltic pump. The contaminant stock solutions were simultaneously pumped (at a rate of 2.7 μL/min) into the mixing chambers using a syringe pump. From the mixing chambers, the solutions were pumped through the columns from bottom to top. Columns 1 and 2 received the contaminants TCE and 1,1,2-TCA, and were operated at a flow rate of 0.5 mL/min. Columns 3 and 4 received the more reactive contaminant 1,1,1-TCA, and were therefore operated at a higher flow rate of 1.25 mL/min to provide a shorter contact time. A summary of the column operating conditions is provided in Table 1.

During the first weeks of operation, the columns received only the inorganic feed solution, in order to allow the pH of the system to equilibrate. Column 3 exhibited clogging problems during the first week and therefore had to be repacked with fresh iron and restarted 6 days later than the other columns. The contaminant feed was initiated on day 19 (day 13 for Column 3). The total operating time was 288 days (282 days for Column 3).

Tracer tests using tritiated water (^3H_2O), as described elsewhere (Vikesland et al., 2003), were conducted during the second week of operation, as well as shortly before shutdown. These tests were carried out to assess whether changes in mean hydraulic residence time or residence time distributions might be occurring.

2.3. Sampling procedures and analytical methods

To determine the contaminant concentrations within the columns, 1 mL liquid samples were removed once a week from every sampling port using a 1 mL glass tuberculin syringe. Samples were then transferred into 2.5 mL autosampler vials. The organic contaminants and their volatile daughter products were analyzed by static headspace gas chromatography (GC) with flame ionization detection (FID). The instrumental system and headspace analysis procedures are described in detail elsewhere (Fennelly and Roberts, 1998). The system was calibrated by analyzing aqueous standards of the contaminants and products by the same

Table 1
Column operating conditions

	Column 1	Column 2	Column 3	Column 4
Feed solution				
$NaHCO_3$	2 mM	2 mM	2 mM	2 mM
SiO_2	(none added)	0.5 mM (continuously)	0.2 mM (days 210–273)	0.5 mM (continuously)
Influent pH	9.2 ± 0.5	9.2 ± 0.5	9.2 ± 0.5	9.2 ± 0.5
Contaminants				
TCE	100 μM (days 19–88, 110–181, 201–215, 253–288) 500 μM (days 182–500)	100 μM (days 19–88, 110–181, 201–215, 253–288) 500 μM (days 182–500)	100 μM (days 176–194)	100 μM (days 182–200)
1,1,2-TCA	100 μM (days 19–60, 89–215, 227–288)	100 μM (days 19–60, 89–215, 227–288)		
1,1,1-TCA			100 μM (days 13–282)	100 μM (days 19–288)
cis-DCE	100 μM (days 216–227)	100 μM (days 216–227)		
Flow rate	0.5 mL/min	0.5 mL/min	1.25 mL/min	1.25 mL/min
Linear velocity[a]	221 cm/day	193 cm/day	397 cm/day	387 cm/day

[a] Average of the linear velocities determined via ^3H_2O tracer tests that were conducted shortly after column startup and before column shutdown.

approach used for the samples. Standards of TCE, 1,1,2-TCA, 1,1,1-TCA, VC, *cis*-DCE, 1,1-DCA, and 2-butyne were prepared and stored in headspace-free 20 mL glass syringes. Standards of *cis*-2-butene, ethane and ethylene were prepared by injecting known amounts of these gases into 2.5 mL autosampler vials containing 1 mL water, following which the vials were immediately sealed.

To obtain profiles of dissolved silica species within the columns, 5 mL aqueous samples were withdrawn through several liquid sampling ports using 10 mL plastic syringes. Silica profiles were initially obtained on a weekly basis, although this sampling frequency was later reduced. Samples were acidified with HNO_3 and were analyzed by atomic absorption spectroscopy (AA), using an N_2O/acetylene flame at a wavelength of 251.6 nm. Details are provided elsewhere (Kohn et al., 2003).

Solid samples for mineral phase characterization were taken on day 68 and after column shutdown. To extract the grains, the columns were brought into an anoxic glovebox (5% H_2, 95% N_2). Several grains were removed through the solid sampling ports and were stored within the glovebox in amber, 2 mL borosilicate glass vials (Kimble Glass, Inc.) filled with liquid obtained from the nearest sampling ports. The precipitates were characterized using X-ray diffraction (XRD) and scanning electron microscopy (SEM).

XRD analysis was performed on samples taken from the port nearest the influent end. In the glovebox, several grains along with some pore liquid were ground using a mortar and pestle until a substantial fraction of the precipitates was removed from the grains into the liquid, as shown by exposure of the bare iron core. The liquid was then transferred onto a low-background silicon (400) wafer and dried overnight. To minimize exposure to air, dried samples were stored in the glove box until analysis, and were transferred to the XRD instrument in an air-tight container under an N_2/H_2 atmosphere. The samples were analyzed using a Philips X'Pert powder X-ray diffractometer operated at a tension of 45 mV and a current of 40 mA. The system was equipped

with a Cu Kα anode as the radiation source ($\lambda = 1.54056$ Å). The scan step size was 0.05° and the scan rate was 5 s/step. Scans from $2\theta = 10$–75° were obtained. The data were collected using the Philips X'Pert Data Collector (v. 2.0) data acquisition software, and they were analyzed by means of the Philips X'Pert HighScore (v. 1.0b) data analysis package.

Samples for SEM analysis were taken from the influent end of both columns, as well as the effluent end of Column 2 on day 68 (day 62 for Column 3). A second set of samples from the influent end was taken at column shutdown. Several grains from each sample were rinsed with deionized water in the glovebox. Once the grains had dried, they were removed from the glovebox and placed in a copper O-ring, and were then embedded in epoxy. After the epoxy had hardened, the samples were polished using sandpaper, and they were carbon-coated to ensure conductivity. The samples were examined using a JEOL 8600 instrument, equipped with an EDAX Genesis System for digital energy dispersive spectroscopy (EDS). The grains were examined by backscattered electron (BSE) imaging and X-ray spectrum mapping. The main focus of the X-ray maps was to locate the silica adsorbed on the grains. In addition, quantitative elemental EDS point analyses were obtained for oxygen, silicon and iron. Because samples were carbon-coated, a quantitative carbon analysis was not possible.

In a prior study of corrosion product formation (Kohn et al., 2005) we have demonstrated that this procedure for precipitate identification successfully avoids oxidation of several redox-active phases. Specifically, results of XRD analyses, as well as selected area electron diffraction (SAED) patterns and electron energy loss (EEL) spectra, accorded with identification of predominant precipitates obtained using in-situ micro-Raman spectroscopy. This indicates that sample drying did not lead to significant losses of the main corrosion products. Furthermore, test samples of carbonate and sulfate green rust prepared for analysis using this approach yielded the expected XRD patterns (Kohn et al., 2005). This confirms that our samples were not significantly oxidized during the time necessary for XRD analysis.

3. Results and discussion

3.1. Hydraulic residence time

Despite the large amount of dissolved silica that adsorbed onto the iron matrix and the formation of iron corrosion products, the mean hydraulic residence times and residence time distributions did not change substantially during the experiments. The breakthrough curves for ^3H_2O obtained from Columns 2 and 3 during tracer experiments at column startup (days 14 and 9, respectively) and shortly before column shutdown (days 273 and 268, respectively) are shown in Fig. 1. It can be seen that the dispersion of the tracer varies slightly between column startup and shutdown, but the mean retention times remain essentially constant. Any differences in contaminant removal efficiency must therefore stem from alterations in reactivity of the iron, rather than from progressive reductions in contact time resulting from diminished porosity as precipitates form.

3.2. Adsorption of dissolved silica species

Under the conditions of this study, the adsorption of dissolved silica species can be viewed as the adsorption of the monomeric form of silicic acid ($Si(OH)_4$) to the iron or the corrosion products. Additional monomers can subsequently adsorb onto the surface-associated species to form a polymeric surface layer (see Kohn et al., 2003 and references therein).

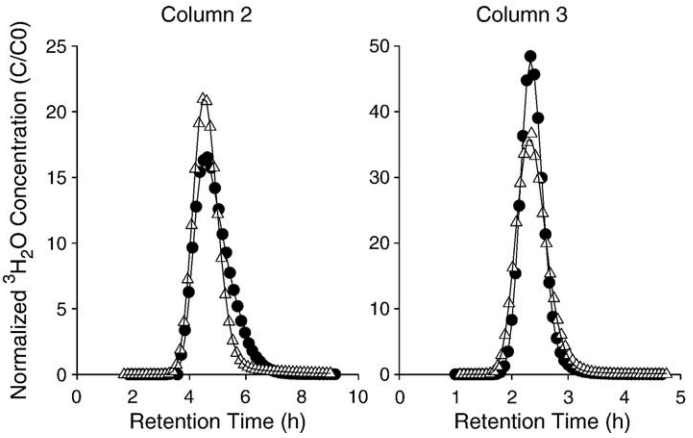

Fig. 1. ^3H_2O breakthrough curves obtained shortly after startup (●) and before shutdown (Δ) in Columns 2 (with dissolved silica, flow rate 0.5 mL/min) and 3 (generally operated in the absence of silica, flow rate 1.25 mL/min). Solid lines are model fits.

The adsorption of dissolved silica species within Columns 2 and 4, which were fed with a 0.5 mM SiO_2 solution, was monitored throughout the entire column operation time. Silica adsorption took place gradually over an extended period. Fig. 2 shows that although slight silica breakthrough occurred during the first 5 days in Column 2 (operated at a flow rate of 0.5 mL/min), substantial breakthrough was evident only after 90 days. Silica uptake continued during the remainder of column operation. This slow uptake of silica is in good agreement with the slow adsorption observed in batch studies using Fisher electrolytic iron (Kohn et al., 2003).

Column 4 (operated at 1.25 mL/min) exhibited some silica breakthrough from the start, and the column approached silica saturation ($C_{effluent}/C_{influent} > 85\%$) after about 190 days. The faster breakthrough observed for this column compared to Column 2 can be attributed to the higher flow rate at which Column 4 was operated. A greater mass of dissolved silica species was pumped through Column 4 per unit time, resulting in a more rapid saturation of the iron. Over

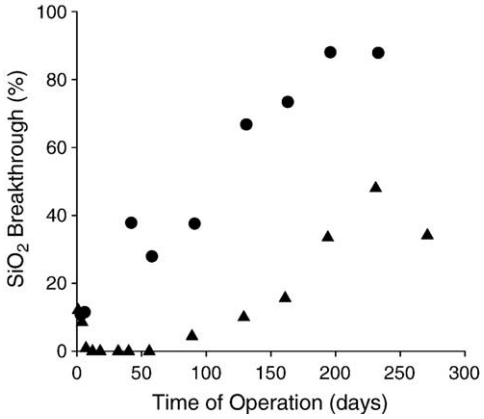

Fig. 2. Breakthrough of SiO_2 (in percent of inlet concentration) in Columns 2 (▲) and 4 (●) as a function of operation time. Both columns were fed with 0.5 mM SiO_2. Column 2 was operated at a flow rate of 0.5 mL/min, Column 4 at 1.25 mL/min.

the duration of these experiments, 82% of the total amount of silica introduced to Column 2 was retained, whereas the total uptake of silica was only 40% in Column 4. Because of the difference in flow rates, however, the absolute amount of silica retained in both columns is similar (80 mmol in Column 2, 98 mmol in Column 4).

Column 3 was fed with 0.2 mM SiO_2 solution from day 210 to day 273 of column operation. Silica breakthrough occurred immediately, and ranged from 33% to 54% (data not shown). The iron matrix of Column 3 was thus less efficient at adsorbing dissolved silica species than the iron matrix of Column 4 (operated at an identical flow rate). This indicates that the precipitates formed under silica-free conditions during the first 210 days in Column 3 may be less effective at adsorbing silica than those initially present. Alternatively, iron corrosion could have occurred at a faster rate when the iron was first exposed to water, forming more precipitates for incorporation or adsorption of dissolved silica species during the early stages of column operation (Column 4) than in later stages (Column 3).

3.3. Effect of silica on the degradation of TCE and 1,1,2-TCA

During most of their operation, Columns 1 and 2 were fed with an influent organohalide concentration of 100 μM TCE and 100 μM 1,1,2-TCA. Previous research has suggested that the effect of silica on the reactivity of iron varies between different classes of compounds (Klausen et al., 2003). Because TCE and 1,1,2-TCA react with iron at comparable rates, they proved suitable for examining differences between the responses of alkyl and vinyl polyhalides toward silica in the same column. To distinguish between inhibitory effects introduced by competition between organohalides for reactive sites from inhibition by silica adsorption, the columns were periodically fed with one contaminant only, or with higher influent concentrations, as indicated in Table 1.

Fig. 3(a) and (b) show typical profiles for TCE and 1,1,2-TCA obtained during single-organohalide experiments in Column 1. The degradation of TCE primarily leads to the formation

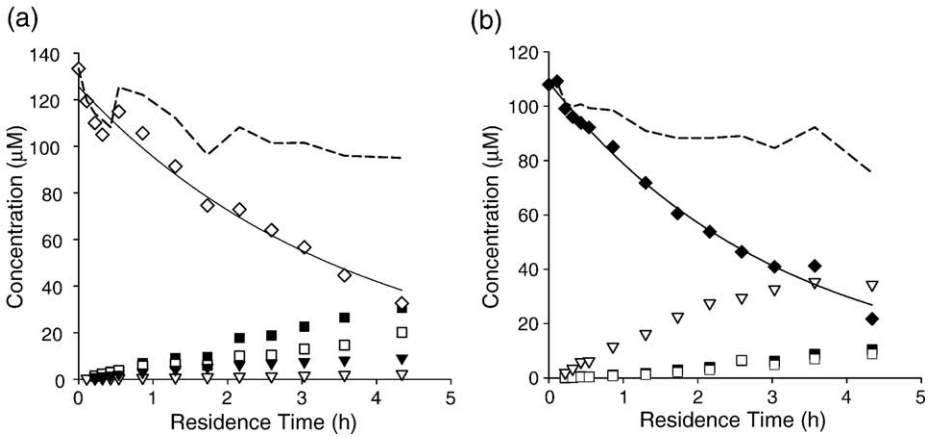

Fig. 3. (a) Degradation profile showing product appearance for TCE in Column 1 on day 61. Symbols represent TCE (◇), vinyl chloride (▽), *cis*-DCE (▼), ethylene (■), ethane (□), mass balance in C_2 equivalents (- - -). The solid line is the pseudo-first-order model fit to the TCE data. (b) Degradation profile showing product appearance for 1,1,2-TCA in Column 1 on day 99. Symbols represent 1,1,2-TCA (◆), vinyl chloride (▽), ethylene (■), ethane (□), mass balance in C_2 equivalents (- - -). The solid line is the pseudo-first-order model fit to the 1,1,2-TCA data.

of ethylene, ethane and *cis*-DCE. Small amounts of VC, as well as trace amounts of trans-DCE and 1,1-DCE (data not shown), were also observed.

The principal reduction product of 1,1,2-TCA is VC. Small amounts of ethylene and ethane were also observed, which could potentially stem from the reduction of VC. The shape of the VC profile, however, suggests that VC is fairly unreactive on the time scale of these experiments.

Reaction rate constants k_{obs} (h^{-1}) were obtained by fitting the contaminant profiles to a pseudo-first-order model with respect to the parent compound concentration. The R^2 values associated with these fits were generally 0.90 or above, and no trends were evident in the residuals. Fig. 4 shows the values of k_{obs} for TCE and 1,1,2-TCA obtained in Columns 1 (no silica) and 2 (with silica) as a function of column operation time. For both compounds, the rate constants obtained in Column 2 were significantly smaller than those measured in Column 1. The inhibitory effect of silica manifested itself promptly; subsequent decreases in reactivity were relatively minor.

Even though silica uptake continued throughout the entire operation time (Fig. 2), neither total loss of reactivity nor the development of a moving passivation front were observed during the course of this study. In the experiments with both contaminants present in the feed solution, the inhibition of k_{obs} by silica (calculated as the average of the ratio k_{obs} (Column 2)/k_{obs} (Column 1) at corresponding operation times for every profile) was $65 \pm 15\%$ for TCE, and $60 \pm 17\%$ for 1,1,2-TCA.

Omission of TCE from the feed solution, however, resulted in an increased rate of 1,1,2-TCA degradation in Column 1, while an increase in the TCE influent concentration to about 500 μM led to a decrease in 1,1,2-TCA reaction rate constants (Fig. 4b) in this column. This indicates that 1,1,2-TCA is subject to competition by TCE as well as to inhibition by silica. The "true" average effect of silica on the rate of 1,1,2-TCA degradation, determined from the single-compound experiments, is 74 ± 8 %. Interestingly, variations of the TCE concentration in the feed solution did not affect the rate of 1,1,2-TCA degradation in Column 2. Omitting 1,1,2-TCA from the feed solution did not result in a change in the TCE reaction rate in either column. TCE is thus not susceptible to interspecies competition by 1,1,2-TCA.

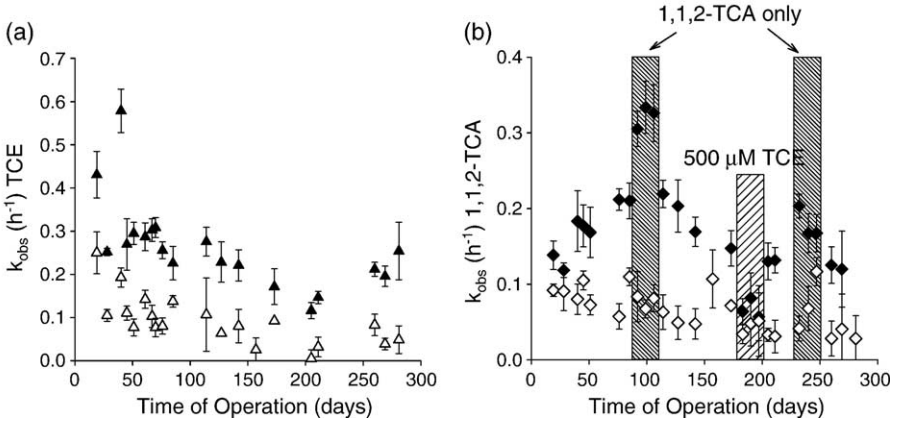

Fig. 4. k_{obs} for the degradation of (a) TCE and (b) 1,1,2-TCA in Columns 1 (solid symbols, no silica) and 2 (open symbols, 0.5 mM SiO_2) over time. The error bars indicate 95% confidence intervals. Both columns were fed with 2 mM $NaHCO_3$ and a contaminant mix of 100 μM TCE and 100 μM 1,1,2-TCA. Column 2 was also continuously fed with 0.5 mM SiO_2. Shaded areas indicate rate constants obtained with 100 μM 1,1,2-TCA only, or with both 100 μM 1,1,2-TCA and 500 μM TCE in the feed solution.

3.4. Effect of silica on the degradation of 1,1,1-TCA

A characteristic profile for 1,1,1-TCA degradation in Column 3 is shown in Fig. 5. The principal reaction product is 1,1-DCA, which itself is not reactive on the time scale of these experiments. Other products observed include ethane and ethylene, as well as the coupling product 2-butyne, which reacts further to form *cis*-2-butene (Fennelly and Roberts, 1998). For clarity of exposition, these products are shown on a smaller scale in the inset of Fig. 5.

The iron matrix was highly reactive toward 1,1,1-TCA, which was fully degraded halfway through the column. 1,1,1-TCA degradation was particularly rapid in the initial portion of Column 3, and the resulting profiles did not adhere very closely to pseudo-first-order kinetics. The reasons for the observed deviation from pseudo-first-order kinetics are not well understood. Possibilities include a higher reactivity toward 1,1,1-TCA of the precipitates formed (under silica-free conditions) at the influent end of Column 3, or insufficient mixing as a result of the higher pumping speed in this column. Adsorption of 1,1,1-TCA onto the iron can be ruled out as an explanation for the deviation from pseudo-first-order kinetics. The good reproducibility of the profiles and the quality of the mass balances showed that steady-state conditions were reached shortly after the introduction of 1,1,1-TCA to the columns. For purposes of comparison with the other columns, we continued to fit the data obtained in Column 3 to pseudo-first-order models. The quality of the fit improved somewhat after 160 days, possibly as a result of the formation of reactive precipitates farther into the column.

Fig. 6(a) shows the rate constants k_{obs} for 1,1,1-TCA degradation obtained in Columns 3 and 4. The reactivity in Column 3 appears to increase during the first 120 days and then stabilize at slightly lower levels prior to the addition of dissolved silica species on day 210. This apparent trend actually represents an artifact caused by the poor adherence to pseudo-first-order decay and the consequent high degree of uncertainty associated with the rate constants within this column. As shown in Fig. 6(b), profiles obtained over the course of the first 210 days of column operation actually exhibited fairly good reproducibility.

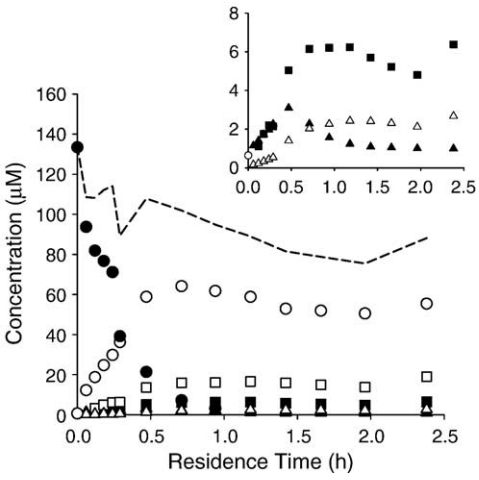

Fig. 5. Degradation profile showing product appearance for 1,1,1-TCA obtained in Column 3 on day 43. Symbols represent 1,1,1-TCA (●), 1,1-DCA (○), *cis*-2-butene (▲), 2-butyne (Δ), ethylene (■), ethane (□), mass balance in C_2 equivalents (- - -). For purposes of visibility, the appearance of *cis*-2-butene, 2-butyne, ethylene and ethane are also shown on a smaller scale in the inset.

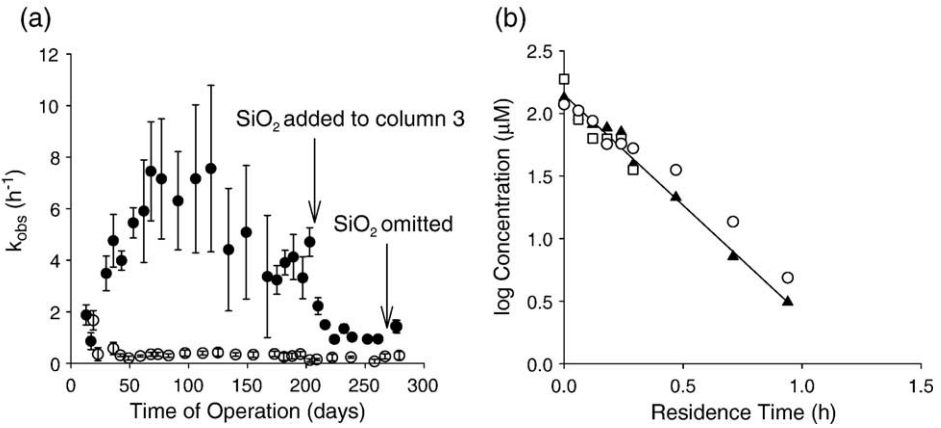

Fig. 6. (a) k_{obs} for the degradation of 1,1,1-TCA in Columns 3 (solid symbols) and 4 (open symbols) over time. The error bars indicate 95% confidence intervals. Column 4 was continuously fed 0.5 mM SiO_2. Column 3 received 0.2 mM SiO_2 from day 210 to day 273. (b) Profiles of 1,1,1-TCA obtained in Column 3 under silica-free conditions, plotted as log concentration, obtained on days 43 (▲), 119 (□) and 175 (○). The solid line represents the pseudo-first-order fit to the profile obtained on day 43.

In contrast to observations for TCE and 1,1,2-TCA, silica initially had little discernible effect on the rate of 1,1,1-TCA reduction. About 4 days after introduction of 1,1,1-TCA to the feed, the reactivity in Column 4 dropped off to very low levels that were nonetheless sustained throughout the duration of the experiment. The average decrease in k_{obs} for 1,1,1-TCA as a result of addition of 0.5 mM SiO_2 to the feed solution was $93 \pm 3\%$. Addition of 100 μM TCE to the feed solution did not result in any measurable decrease in the reaction rate constant for 1,1,1-TCA for either column. Unlike 1,1,2-TCA, 1,1,1-TCA does not appear to be subject to interspecies competition by TCE.

The two alkyl halide species seemed to be affected by silica to a greater extent than the vinyl halide species. We speculate this may reflect stronger interaction between TCE and reactive sites than between 1,1,2-TCA or 1,1,1-TCA and reactive sites. Chlorinated ethylenes have been shown to adsorb strongly onto iron, carbon impurities or non-reactive sites therein (Burris et al., 1998). Chlorinated ethanes may be less likely to adsorb to Lewis acid surface sites, because the absence of a π-bond makes electron donor–acceptor interactions that may play a role in sorption less likely (Arnold and Roberts, 2000).

Starting on day 210, Column 3 received a feed solution containing 0.2 mM dissolved SiO_2. The rate constants continuously dropped off during the ensuing 2 weeks before stabilizing at values around 1 h^{-1} (Fig. 6(a)). This corresponds to a reactivity loss of about 70% compared to the reaction rate constants obtained just prior to silica addition. Even though this loss is substantial, the reactivity of Column 3 is still high compared to Column 4, which had continuously been fed with 0.5 mM SiO_2. The iron reactivity toward 1,1,1-TCA may thus be a function of the dissolved silica species concentration in the feed solution. It is also possible that Column 3 may have maintained higher levels of reactivity because dissolved silica species were retained less efficiently, as discussed above. Dissolved silica species were omitted from the feed solution of Column 3 on day 273, at which point the reactivity rebounded slightly but not completely. Because clogging of sampling ports forced us to terminate the experiment shortly thereafter, we cannot establish whether the iron matrix of Column 3 could have eventually recovered its full reactivity.

3.5. Effect of silica on product distribution

A comparison of the distribution of products encountered in silica-free and silica-containing columns is shown in Fig. 7. The data shown were obtained during single compound experiments. The product ratios were generally constant at each point within the columns as well as over time.

Silica had no discernible effect on the distribution of products arising from the alkyl polyhalides 1,1,2-TCA and 1,1,1-TCA. The degradation of these compounds was retarded by the presence of silica in Columns 2 and 4, but pathways and branching ratios remained unaffected by silica. In the case of TCE, however, the product distribution shifted from ethylene in favor of ethane and *cis*-DCE in the silica-containing Column 2. The higher concentration of *cis*-DCE cannot be attributed to a slower rate of *cis*-DCE degradation in Column 2, because a test of *cis*-DCE degradation (in the absence of TCE) showed that this compound reacts at negligible rates in both columns. The higher *cis*-DCE concentrations in Column 2 must therefore result from a shift in the product branching ratio. Sorbed silica could either block some reactive sites for TCE, causing it to react with different sites, or it may alter the properties of the present sites leading to less complete dechlorination. The lack of iron reactivity toward *cis*-DCE in the present study may stem from competition from residual TCE, as other researchers have reported that *cis*-DCE can be reduced by Connelly iron (VanStone et al., 2004).

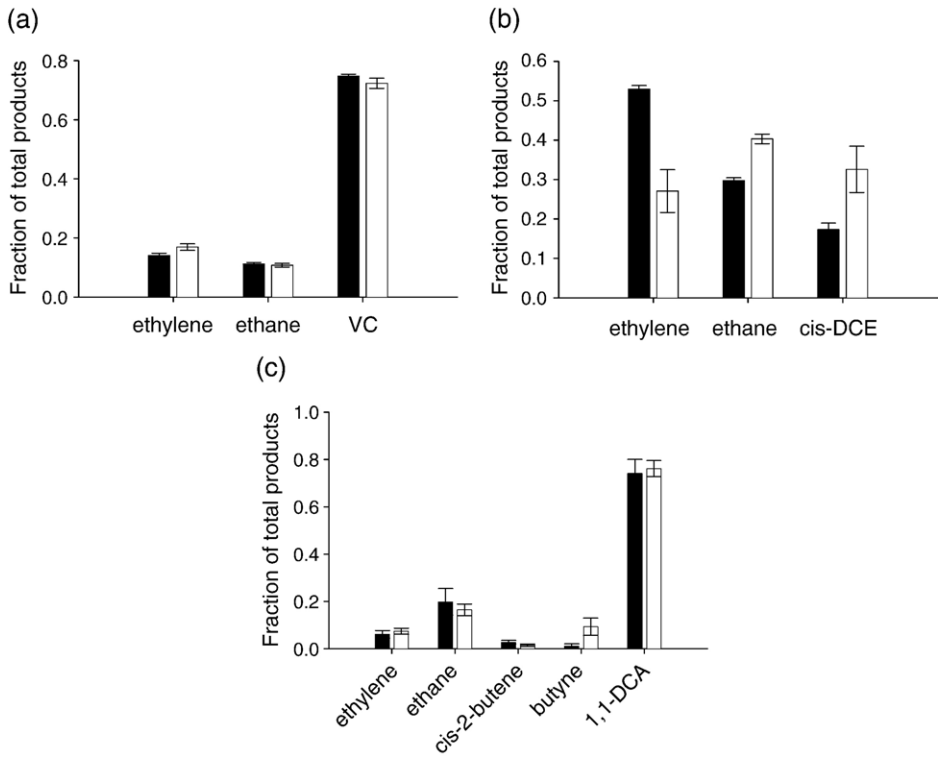

Fig. 7. Distribution of the main degradation products of (a) 1,1,2-TCA and (b) TCE in Columns 1 (black bars, no silica) and 2 (white bars, 0.5 mM dissolved silica) from single compound experiments. Error bars indicate one standard deviation. (c) Distribution of the main degradation products of 1,1,1-TCA in Columns 3 (black bars, no silica) and 4 (white bars, 0.5 mM dissolved silica). Error bars indicate one standard deviation.

3.6. Precipitate characterization

Several researchers have observed that the presence of dissolved silica species can inhibit or promote the formation of different mineral phases (Anderson and Benjamin, 1985; Hansen et al., 1994; Mayer and Jarrell, 1996). We therefore expect to see qualitative disparities in the precipitates formed in Columns 1 and 3 compared to the silica-fed Columns 2 and 4. A quantitative analysis of differences in the abundance of corrosion products is not feasible because of the high uncertainty associated with how effectively the precipitates are removed from the grains during sample preparation.

XRD analyses of precipitates obtained at column shutdown showed that the main crystalline phases in all samples were carbonate green rust ($[Fe_4^{2+}Fe_2^{3+}(OH)_{12}][CO_3 \cdot 2H_2O]$) and magnetite ($Fe_3O_4$) or maghemite ($\gamma$-$Fe_2O_3$). The latter two mineral phases are difficult to distinguish by XRD. The XRD pattern obtained from a sample of Column 1 (Fig. 8) also contained iron carbonate hydroxide ($Fe(II)_{1.8}Fe(III)_{0.2}(OH)_{2.2}CO_3$), a redox-active phase that is discussed in more detail elsewhere (Erdös and Altorfer, 1976; Kohn et al., 2005). Trace amounts of additional crystalline mineral phases may be present in our samples, but did not accumulate to levels detectable by XRD. Poorly crystalline phases such as ferrihydrite ($Fe_5HO_8 \cdot 4H_2O$) have been found by transmission electron microscopy to be present in PRBs containing Peerless iron (Furukawa et al., 2002). Ferrihydrite and other amorphous iron (hydr)oxide phases may be present in our columns, but cannot be identified by XRD.

The absence of iron carbonate hydroxide in Columns 2–4 suggests that the addition of dissolved silica species may prevent this phase from forming. The silica-free operation period of Column 3 may not have been sufficiently long to produce enough iron carbonate hydroxide for identification by XRD. Alternatively, the higher flow rate in Column 3 may have been less favorable for the formation of this phase.

On day 68 (day 62 for Column 3), as well as after column shutdown, grain samples were taken for analysis by SEM. Images and elemental maps were obtained to examine the morphology of the precipitates, as well as their elemental composition. Fig. 9(a) shows a close-

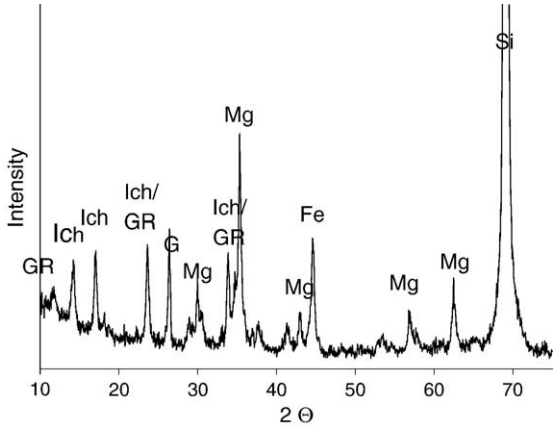

Fig. 8. XRD pattern of the precipitates formed on a sample from Column 1 (no silica) obtained after column shutdown. Green rust (GR), iron carbonate hydroxide (Ich) and magnetite/maghemite (Mg) are corrosion products. Also evident are peaks from metallic iron (Fe), the low-background silicon (400) wafer (Si), and graphite (G), a common cast iron impurity.

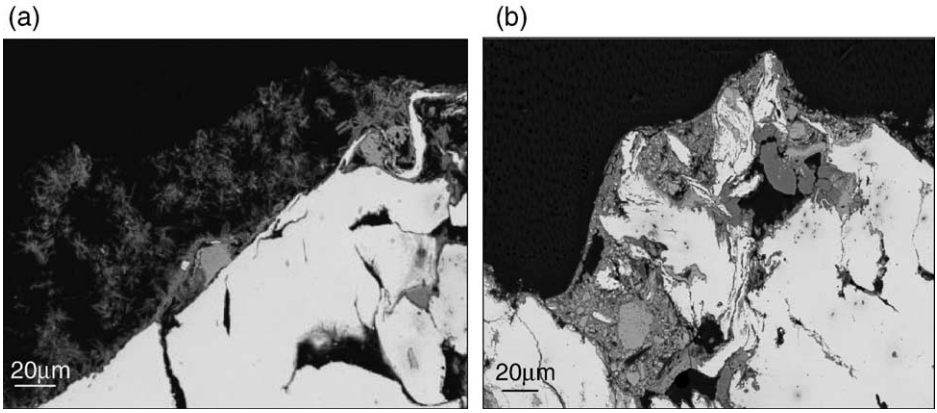

Fig. 9. (a) SEM image of a grain sample taken from the influent end of Column 1 (no silica) after column shutdown. Fine needles have formed on the grain surface. (b) SEM image of a grain sample taken from the influent end of Column 2 (0.5 mM dissolved silica) after column shutdown. No needle-like structures are evident.

up of parts of the iron core (lightest areas) and precipitate layer (gray areas) of a grain from the influent end of Column 1, taken after shutdown. The grain is covered with a layer of small needles or plates adjacent to the iron core. This feature was prominent in all samples from Column 1, and to a lesser extent in samples from Column 3. Plate-like structures have been associated with green rust (Legrand et al., 2001; Williams and Scherer, 2001) and needle-like structures with iron carbonate hydroxide (Kohn et al., 2005). In samples from the influent end of Columns 2 and 4, a needle- or plate-like structure was only found in a very few spots on the grain surface. The precipitate layer in these two columns was of a more compact and grainy nature, as can be seen in an image of a sample from Column 2 shown in Fig. 9(b). A grain sample from the effluent end of Column 2 showed very little weathering and no needle-like structures. Little change was observed between the sets obtained at shutdown relative to their appearance on day 68. The weathering of the grains thus seems to occur very slowly.

Quantitative elemental EDS point analyses were performed on several spots of the metal core and the precipitate layers of the samples taken from Columns 1 and 2 after column shutdown. Table 2 summarizes the results obtained from these analyses. As observed in a previous study (Kohn et al., 2005), the precipitates on the grains from silica-containing Column 2 are strongly enriched in silicon, whereas the precipitates formed in the silica-free Column 1 are depleted in Si compared to the iron core. This can also be seen from elemental maps of samples from Columns 1 and 2, shown in Fig. 10. The precipitates on the Si map of Column 1 appear slightly darker than the iron core. EDS point analyses showed that the iron core in this sample contains about 6% Si, whereas the precipitates contain only 0–2% Si (Table 2). In a grain sample from Column 2, the precipitates show up bright in the Si map, indicating a relatively high Si concentration.

Table 2
Distribution of elements in the iron core and the precipitate layers

	O (%)	Si (%)	Fe (%)
Iron core	9–10	6–6.56	84–85
Precipitates Column 1	62–66	0–2	33–37
Precipitates Column 2	65–67	10–18	18–25

The data represent a range over at least three locations analyzed.

According to EDS point analyses, the Si content is 10–18%. In spite of the high Si content in samples from Column 2, no Si-containing mineral phases were identified by XRD. Dissolved silica species are thus either being adsorbed onto or incorporated into original and newly formed precipitates, or they precipitate as an amorphous phase not detectable by XRD.

The impact of silica on iron reactivity can be attributed to a combination of effects. Differences in the prevalent precipitate phases, namely the absence of iron carbonate hydroxide, may have led to the observed significant losses in iron reactivity. A previous study using Master Builder iron (Kohn et al., 2005), however, revealed that even columns in which large amounts of iron carbonate hydroxide had been formed lost some reactivity upon addition of dissolved silica species to the feed solution. Adsorption of dissolved silica species to previously formed precipitates, as well as incorporation of dissolved silica species into newly formed precipitates, therefore also leads to a decrease in reactivity.

3.7. Comparison with Master Builder iron

In a previous study, we investigated the long-term reactivity of Master Builder iron toward TCE under different feed solution conditions (Klausen et al., 2003). Two columns (Columns D and J) were fed with 2 mM $NaHCO_3$ and 100 μM TCE at an influent pH of 9.2. The reactivity data from these two columns are thus directly comparable to the data obtained from Column 1 in the present study, because 1,1,2-TCA does not seem to affect TCE degradation. Fig. 11 shows a comparison of the pseudo-first-order rate constants obtained over 300 days in both studies. Master Builder iron columns started out about twice as reactive as the Connelly iron in Column 1. Their reactivity, however, continuously dropped off to eventually attain values similar to the Connelly iron Column 1 after 250 days. The Connelly iron was initially less reactive, but maintained a more stable level of reactivity over the entire operation time (Fig. 4a).

Grains from the Master Builder iron columns were analyzed by XRD and SEM after 475 days of exposure (Kohn et al., 2005). Compared to the Connelly iron grains after 288 days, the Master Builder iron grains were much more heavily weathered, and the observed needle-like structures attributed to iron carbonate hydroxide were much larger. The increased amount of corrosion products is consistent with the TCE data that suggests Master Builder iron grains initially corrode more readily than Connelly iron grains, contributing to the initially higher reactivity and more dramatic subsequent loss observed in the Master Builder iron columns. The differences in weathering between the two iron types may be related to differences observed in the scale on the grain surfaces. Master Builder iron grains have a compact, fayalite (Fe_2SiO_4)-containing scale. The location of the scale and indications of scale breakdown were evident in SEM images (Kohn et al., 2005). Connelly iron grains, in contrast, have no easily identifiable scale (see Figs. 9 and 10).

3.8. Conclusions and implications for barrier design

The presence of dissolved silica species in groundwater has the potential to compromise the reactivity of a PRB toward chlorinated solvents. Even though the adsorption of silica species in a flow-through system is a slow process, its impact on iron reactivity toward chlorinated hydrocarbons is almost immediate. PRBs in regions of high concentrations of dissolved silica species may not fail immediately, but their reactivity may be substantially compromised.

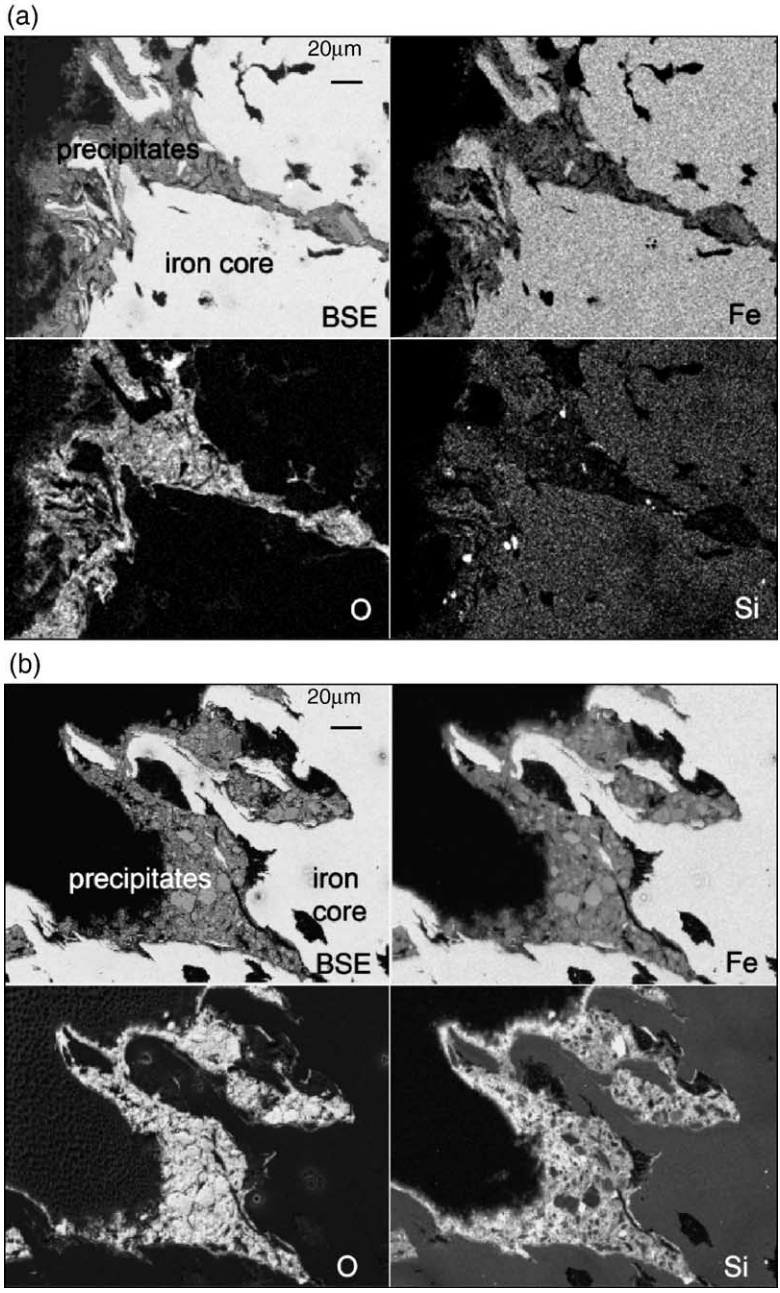

Fig. 10. (a) Elemental map of a sample taken from the influent end of Column 1 (no silica) after column shutdown. The precipitates are depleted in Si compared to the iron core. (b) Elemental map of a sample taken from the influent end of Column 2 (0.5 mM dissolved silica) after column shutdown. The precipitate layer is heavily enriched in Si. BSE=backscattered electron image, Fe=iron, O=oxygen, Si=silicon. Brighter regions correspond to higher concentrations of the element in question.

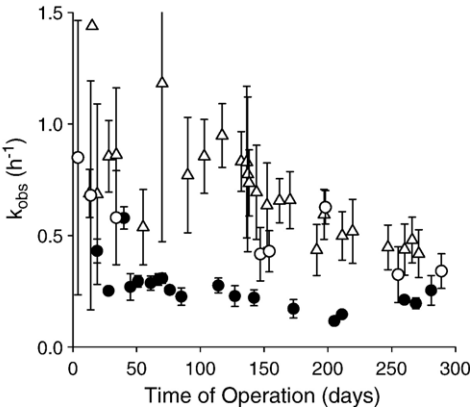

Fig. 11. Comparison of k_{obs} for the degradation of TCE in two Master Builder iron columns (Δ and ○) and a Connelly iron column (●) over time. The error bars indicate 95% confidence intervals. All columns received 2 mM $NaHCO_3$ and an influent concentration of 100 μM TCE.

The inhibitory effect is not only dependent on the concentration of dissolved silica species in the feed solution, but also on the class of organohalide, as well as the type of iron used for the reactive matrix. In addition, the adsorption of silica species to the iron matrix can lead to impaired PRB performance by shifting the product distribution toward less desirable reaction products. Problems that may result if such effects were overlooked in designing PRBs could be alleviated if these factors were recognized during bench-scale tests. Consideration should be given in such cases either to including silica species in simulated groundwater, or better yet to employing actual site groundwater during such tests.

Acknowledgements

This material is based upon work supported by the National Science Foundation (Grant no. CHE-0089168) as part of the Collaborative Research Activities in Environmental Molecular Science in Environmental Redox-Mediated Dehalogenation Chemistry at Johns Hopkins University. The authors would like to thank Connelly-GPM, Inc. for donating the iron. The help of Ken Livi with the SEM studies is greatly appreciated. Finally, we would like to express out appreciation for the suggestions provided by two anonymous reviewers.

References

Agrawal, A., Tratnyek, P.G., 1996. Reduction of nitroaromatic compounds by zero-valent iron metal. Environ. Sci. Technol. 30, 153–160.

Anderson, P.R., Benjamin, M.M., 1985. Effects of silicon on the crystallization and adsorption properties of ferric oxides. Environ. Sci. Technol. 19, 1048–1053.

Arnold, W.A., Roberts, A.L., 2000. Pathways and kinetics of chlorinated ethylene and chlorinated acetylene reaction with Fe(O) particles. Environ. Sci. Technol. 34, 1794–1805.

Blowes, D.W., Ptacek, C.J., Jambor, J.L., 1997. In-situ remediation of Cr(VI)-contaminated groundwater using permeable reactive walls: laboratory studies. Environ. Sci. Technol. 31, 3348–3357.

Burris, D.R., Allen King, R., Manoranjan, V.S., Campbell, T.J., Loraine, G.A., Deng, B., 1998. Chlorinated ethene reduction by cast iron: sorption and mass transfer. J. Environ. Eng., 1012–1019.

Cantrell, K.J., Kaplan, D.I., Wietsma, T.W., 1995. Zero-valent iron for the in situ remediation of selected metals in groundwater. J. Hazard. Mater. 42, 201–212.

Connelly-GPN, Inc., http://www.connellygpm.com/wtiron.html (accessed in March 2004).
Davies, C.C., Chen, H.W., Edwards, M., 2002. Modeling silica sorption to iron hydroxide. Environ. Sci. Technol. 36, 582–587.
Deng, B., Shaodong, H., Burris, D.R., 1998. Effect of iron corrosion inhibitors on trichloroethylene reduction. In: Wickramanayake, G.B., Hinchee, R.E. (Eds.), The First International Conference on Remediation of Chlorinated and Recalcitrant Compounds. Physical, Chemical, and Thermal Technologies. Remediation of Chlorinated and Recalcitrant Compounds. Batelle Press, Monterey, CA, pp. 341–346.
Erbs, M., Bruun, H.C., Olsen, C.E., 1999. Reductive dechlorination of carbon tetrachloride using iron(II) iron(III) hydroxide sulfate (green rust). Environ. Sci. Technol. 33, 307–311.
Erdös, E., Altorfer, H., 1976. Ein dem Malachit ähnliches basisches Eisenkarbonat als Korrosionsprodukt von Stahl. Werkst. Korros. 27, 304–312.
Fennelly, J.P., Roberts, A.L., 1998. Reaction of 1,1,1-trichloroethane with zero-valent metals and bimetallic reductants. Environ. Sci. Technol. 32, 1980–1988.
Furukawa, Y., Kim, J.-W., Watkins, J., Wilkin, R.T., 2002. Formation of ferrihydrite and associated iron corrosion products in permeable reactive barriers of zero-valent iron. Environ. Sci. Technol. 36, 5469–5475.
Gillham, R.W., O'Hannesin, S.F., 1994. Enhanced degradation of halogenated aliphatics by zero-valent iron. Ground Water 32, 958–967.
Gu, B., Liang, L., Dickey, M.J., Yin, X., Dai, S., 1998. Reductive precipitation of uranium (VI) by zero-valent iron. Environ. Sci. Technol. 32, 3366–3373.
Hansen, H.C.B., Wetche, T.P., Raulundrasmussen, K., Borggaard, O.K., 1994. Stability-constants for silicate adsorbed to ferrihydrite. Clay Min. 29, 341–350.
Klausen, J., Tröber, S.P., Haderlein, S.B., Schwarzenbach, R.P., 1995. Reduction of substituted nitrobenzenes by Fe(II) in aqueous mineral suspensions. Environ. Sci. Technol. 29, 2396–2404.
Klausen, J., Ranke, J., Schwarzenbach, R.P., 2001. Influence of solution composition and column aging on the reduction of nitroaromatic compounds by zero-valent iron. Chemosphere 44, 511–517.
Klausen, J., Vikesland, P.J., Kohn, T., Burris, D.R., Ball, W.P., Roberts, A.L., 2003. Longevity of cast iron in groundwater treatment processes: solution composition effects on reactivity towards organohalides and nitroaromatic compounds. Environ. Sci. Technol. 37, 1208–1218.
Kohn, T., Kane, S.R., Fairbrother, D.H., Roberts, A.L., 2003. Investigation of the inhibitory effect of silica on the degradation of 1,1,1-trichloroethane by granular iron. Environ. Sci. Technol. 37, 5806–5812.
Kohn, T., Livi, K.J.T., Roberts, A.L., Vikesland, P.J., 2005. Longevity of granular iron in groundwater treatment processes: corrosion product development. Environ. Sci. Technol. 39, 2867–2879.
Lee, W., Batchelor, B., 2002a. Abiotic reductive dechlorination of chlorinated ethylenes by iron-bearing soil minerals: 1. Pyrite and magnetite. Environ. Sci. Technol. 36, 5147–5154.
Lee, W., Batchelor, B., 2002b. Abiotic reductive dechlorination of chlorinated ethylenes by iron-bearing soil minerals: 2. Green rust. Environ. Sci. Technol. 36, 5348–5354.
Legrand, L., Abdelmoula, M., Gehin, A., Chausse, A., Genin, J.-M.R., 2001. Electrochemical formation of a new Fe(II)–Fe(III) hydroxy-carbonate green rust: characterisation and morphology. Electrochim. Acta 46, 1815–1822.
Mayer, T.D., Jarrell, W.M., 1996. Formation and stability of iron(II) oxidation products under natural concentrations of dissolved silica. Water Res. 30, 1208–1214.
O'Loughlin, E.J., Kelly, S.D., Cook, R.E., Csencsits, R., Kemner, K.M., 2003. Reduction of uranium(VI) by mixed iron(II)/iron(III) hydroxide (green rust): formation of UO_2 nanoparticles. Environ. Sci. Technol. 37, 721–727.
Ritter, K., Odziemkowski, M.S., Gillham, R.W., 2002. An in-situ study of the role of surface films on granular iron in the permeable iron wall technology. J. Contam. Hydrol. 55, 87–111.
Ritter, K., Odziemkowski, M.S., Simpgraga, R., Gillham, R.W., Irish, D.E., 2003. An in situ study of the effect of nitrate on the reduction of trichloroethylene by granular iron. J. Contam. Hydrol. 65, 121–136.
Sass, B., Gavaskar, A.R., Yoon, W.-S., 2001. Analysis of corrosion compounds associated with permeable reactive barriers and their impact on barrier longevity. Innovative Strategies for the Remediation of Chlorinated Solvents and DNAPLs in the Subsurface, San Diego, CA, 1161–1166.
Sastri, V.A., 1998. Corrosion Inhibitors. Principles and Applications. John Wiley and Sons Ltd., West Sussex, England.
Schlicker, O., Ebert, M., Fruth, M., Weidner, M., Wüst, W., Dahmke, A., 2000. Degradation of TCE with iron: the role of competing chromate and nitrate reduction. Ground Water 38, 403–409.
Sigg, L., Stumm, W., 1981. The interaction of anions and weak acids with the hydrous goethite (α-FeOOH) surface. Colloids Surf. 2, 101–117.
Sivavec, T.M., Horney, D.P., 1997. Reduction of chlorinated solvents by iron(II) minerals. 213th National Meeting of the American Chemical Society. Abstract of Papers. American Chemical Society, Washington, DC, pp. 115–117.

Su, C., Puls, R.W., 1999. Kinetics of trichloroethene reduction by zerovalent iron and tin: pretreatment effect, apparent activation energy, and intermediate products. Environ. Sci. Technol. 33, 163–168.

Su, C., Puls, R.W., 2001a. Arsenate and arsenite removal by zerovalent iron: kinetics, redox transformation, and implications for in situ groundwater remediation. Environ. Sci. Technol. 35, 1487–1492.

Su, C., Puls, R.W., 2001b. Arsenate and arsenite removal by zerovalent iron: effects of phosphate, silicate, carbonate, borate, sulfate, chromate, molybdate, and nitrate, relative to chloride. Environ. Sci. Technol. 35, 4562–4568.

Su, C., Puls, R.W., 2003. In situ remediation of arsenic in simulated groundwater using zerovalent iron: laboratory column tests on combined effects of phosphate and silicate. Environ. Sci. Technol. 37, 2582–2587.

Swedlund, P.J., Webster, J.G., 1999. Adsorption and polymerisation of silicic acid on ferrhydrite, and its effects on arsenic adsorption. Water Res. 33, 3413–3422.

VanStone, N.A., Focht, R.M., Mabury, S.A., Lollar, B.S., 2004. Effect of iron type on kinetics and carbon isotopic enrichment of chlorinated ethylenes during abiotic reduction of Fe(0). Ground Water 42, 268–276.

Vikesland, P.J., Klausen, J., Zimmermann, H., Roberts, A.L., Ball, W.P., 2003. Longevity of cast iron in groundwater treatment processes: changes in solute transport properties over time. J. Contam. Hydrol. 64, 3–33.

Wilkin, R.T., McNeil, M.S., 2003. Laboratory evaluation of zero-valent iron to treat water impacted by acid mine drainage. Chemosphere 53, 715–725.

Williams, A.G.B., Scherer, M.M., 2001. Kinetics of Cr(VI) reduction by carbonate green rust. Environ. Sci. Technol. 35, 3488–3494.